JOURNAL OF THE ROYAL SOCIETY Interface

J. R. Soc. Interface (2011) **8**, 1192–1203
doi:10.1098/rsif.2010.0680
Published online 3 February 2011

Nanostructured glass–ceramic coatings for orthopaedic applications

Guocheng Wang[1], Zufu Lu[1], Xuanyong Liu[2], Xiaming Zhou[2], Chuanxian Ding[2] and Hala Zreiqat[1,*]

[1]*Biomaterials and Tissue Engineering Research Unit, School of AMME, University of Sydney, Sydney 2006, Australia*
[2]*Shanghai Institute of Ceramics, Chinese Academy of Sciences, Shanghai 200050, People's Republic of China*

Glass–ceramics have attracted much attention in the biomedical field, as they provide great possibilities to manipulate their properties by post-treatments, including strength, degradation rate and coefficient of thermal expansion. In this work, hardystonite (HT; $Ca_2ZnSi_2O_7$) and sphene (SP; $CaTiSiO_5$) glass–ceramic coatings with nanostructures were prepared by a plasma spray technique using conventional powders. The bonding strength and Vickers hardness for HT and SP coatings are higher than the reported values for plasma-sprayed hydroxyapatite coatings. Both types of coatings release bioactive calcium (Ca) and silicon (Si) ions into the surrounding environment. Mineralization test in cell-free culture medium showed that many mushroom-like Ca and phosphorus compounds formed on the HT coatings after 5 h, suggesting its high acellular mineralization ability. Primary human osteoblasts attach, spread and proliferate well on both types of coatings. Higher proliferation rate was observed on the HT coatings compared with the SP coatings and uncoated Ti-6Al-4V alloy, probably due to the zinc ions released from the HT coatings. Higher expression levels of Runx2, osteopontin and type I collagen were observed on both types of coatings compared with Ti-6Al-4V alloy, possibly due to the Ca and Si released from the coatings. Results of this study point to the potential use of HT and SP coatings for orthopaedic applications.

Keywords: plasma spray; orthopaedic; titanium alloy; nanostructure; osteogenic genes; glass–ceramic

1. INTRODUCTION

Titanium alloy (Ti-6Al-4V) is widely used in orthopaedic applications including artificial hip joints, bone plates and dental implants because of its excellent mechanical properties [1]. However, the main drawback of Ti-6Al-4V implants is the formation of dense fibrous tissue at the implant–bone interface due to its bioinertness [2], which jeopardizes the stability of prostheses, leading to the premature failure of devices. Coating Ti-6Al-4V implants with a bioactive coating is an effective way to solve this problem, as the coating can accelerate new-bone formation at the bone–implant interface, leading to strong anchorage of the device material in surrounding bone tissue and thus extending the life time of the implants. Various surface modification techniques have been used, including sol–gel, plasma spray, biomimetic deposition, pulsed laser deposition and ion beam techniques [3]. Plasma spray is by far the most-established commercial technique, owing to its high deposition rate, thick deposit, low capital and operation cost [4], together with the fact that the rough surfaces of plasma-sprayed coatings are favourable for bone fixation [5]. Plasma-sprayed hydroxyapatite (HAp) coatings have been commercialized and widely used in hip joint replacements owing to the chemical similarity of HAp to the inorganic component of human bones. However, the main concern with HAp coating is its low bonding strength to the underlying Ti-6Al-4V resulting from the mismatch of their thermal expansion coefficients, which will raise the delamination risk of the coatings. Once delamination occurs, the fragments of the coatings will promote inflammation and resultant osteolysis, thus compromising the long-term stability of the Ti-6Al-4V implants [6].

An alternative method is to coat the implants with $CaO–SiO_2$-based bioglass whose bioactivity has been well documented *in vitro* [7–11] and *in vivo* [12,13]. However, most plasma-sprayed bioglass coatings fail owing to their weak interfacial bonding with Ti-6Al-4V alloy resulting from higher thermal expansion coefficient ($14–15 \times 10^{-6}\,K^{-1}$ [14]) relative to that of the alloy ($8.4–8.8 \times 10^{-6}\,K^{-1}$ [15]) [16]. High degradation rate is another barrier for using bioglass as implant coatings. However, it is known that the release of calcium (Ca) and silicon (Si) ions enhances osteoblast attachment, proliferation and differentiation [17–20],

*Author for correspondence (hzreiqat@usyd.edu.au).

Received 1 December 2010
Accepted 14 January 2011

and promotes bone formation [11,21]. Therefore, designing $CaO–SiO_2$-based coatings with a limited release of Ca and Si ions, which will not compromise the long-term stability of the coatings, would result in coatings with enhanced bioactivity. In our previous work, we reported that hardystonite (HT) or sphene (SP) ceramics, produced by the addition of ZnO [22] or TiO_2 [23], respectively, into the $CaO–SiO_2$ system, possess better chemical stability compared with $CaSiO_3$ ceramics. Additionally, their thermal expansion coefficients ($11.2 \times 10^{-6}\,K^{-1}$ for HT [24]; $6 \times 10^{-6}\,K^{-1}$ for SP [25]) are closer to that of Ti-6Al-4V alloys, implying that higher bonding strength should be obtained. Therefore, it is plausible to suggest that HT and SP would be suitable candidate coatings for orthopaedic applications.

Glass–ceramics consisting of both amorphous and crystalline phases have attracted great interest in the biomaterials field. One of their advantages over bioglass is that they provide great possibilities to manipulate their properties, including strength, resistance to abrasion and coefficient of thermal expansion [26]. Their degradation rate or ion release behaviour can be tailored by controlling the extent of crystallization using post-heat treatments [26,27]. Plasma spray technique has advantages for producing glass–ceramics. Firstly, it yields temperatures up to 12 000 K in the core region of a plasma jet. Secondly, the cooling rate of the plasma spray process is in excess of 10^6–$10^7{}^\circ C\,s^{-1}$ [3]. Under these thermal conditions, the feeding powders are completely or partially melted in the plasma jet, depending on the powder properties and the processing parameters. The melted powders undergo rapid solidification under this high cooling rate. As the high cooling rate can suppress nucleation from the melts and the growth of crystallites, properly controlling the processing condition can keep both glass and crystalline phases in the coatings, thus forming glass–ceramic coatings. Additionally, it is worth noting that appropriately adjusting processing parameters can endow plasma-sprayed coatings with nanostructures [28,29], which have been proved to be beneficial for their biocompatibility [30–33].

In the present study, glass–ceramic HT and SP coatings with nanostructured surface were deposited on Ti-6Al-4V alloy using the plasma spray technique. Their potential use as biomedical coatings for orthopaedic applications was explored in this work.

2. MATERIAL AND METHODS

2.1. Powder synthesis and coating fabrication

The HT ($Ca_2ZnSi_2O_7$) and SP ($CaTiSiO_5$) powders were synthesized by high temperature solid reaction. Briefly, reagent grade $CaCO_3$, ZnO and SiO_2 powders were mixed in a 2 : 1 : 2 molar proportion for synthesizing HT ceramic powders; $CaCO_3$, TiO_2 and SiO_2 powders were mixed in a 1 : 1 : 1 molar proportion for synthesizing SP ceramic powders. After drying, the mixed powders were sintered at 1200°C for 3 h (HT powder) and at 1290°C for 6 h (SP powder). Then, the as-sintered powders were ground and sieved. Powders with particle size below 75 μm were made more flowable by reconstitution with 6 wt% poly(vinyl alcohol) (PVA) solution for plasma spraying. The process of reconstitution of the powders can be briefly described as follows: powders were placed in a mortar, and PVA solution was dropwise added into the powders during gentle grinding. After thorough mixing, powders were dried at 80°C for 12 h. The reconstituted powders were finally sieved using 80 mesh sieves. Those below 80 mesh (less than 177 μm) were used for plasma spraying.

An atmospheric plasma spray system (Sulzer Metco, Switzerland) was applied to deposit HT and SP coatings on commercial Ti-6Al-4V discs (Baoji Junhang Metal Material Co., Ltd) of 15 mm in diameter and 1 mm in thickness. Before plasma spraying, the discs were ultrasonically cleaned in absolute ethanol and grit-blasted with alumina sands. The processing parameters, which were optimized with respect to the phase composition of the coatings, are described as follows: argon (40 slpm) and hydrogen (12 slpm) were used as primary and auxiliary plasma forming gases, respectively. The powder feeding rate was about $20\,g\,min^{-1}$ using argon (3.5 slpm) as a carrying gas. The plasma arc current and voltage were 600 A and 70 V, respectively. The spraying distance was fixed at 100 mm. The diameter of feeding tube was 1.8 mm, powder feeding angle was 90°; the velocity of the torch was $10\,mm\,s^{-1}$, the time interval between adjacent passes was about 5 s; the overall number of cycles was 20. After spraying, coating samples were cut into halves and mounted in epoxy resin with the new cutting plane facing down. The cross section was ground with SiC abrasive papers and polished using 0.3 μm Al_2O_3 polishing paste. The surface of the coating samples used for micro-indentation tests was also ground and polished.

The morphology of the surface and the cross section of the coatings were examined by field emission scanning electron microscopy (SEM, Zeiss EVO 50). The phase composition of the coatings was analysed using X-ray diffraction (XRD, Siemens D6000, Germany) with Cu Kα1 radiation at a step size of 0.02°. Data were obtained from 15 to 75° (2θ) at a scanning rate of $4^\circ\,min^{-1}$. The surface roughness (R_a) was measured by a surface profilometer (Hommelwerke T8000-C, Germany). Three samples for each type of coatings were tested and the roughness values of five different tracks on each sample were recorded. The R_a values were expressed as mean ± standard deviation (s.d.) ($n = 15$).

2.2. Bonding strength and micro-hardness

The tensile bonding strength between coating and substrate was measured in accordance with ASTM C-633-79. The testing procedure can be found in our previous work [32]. Five samples were tested independently for each type of coatings and the results were reported as mean ± s.d.

The micro-hardness of the coatings was tested on polished coating surfaces using a Shimadzu micro hardness tester (Shimadzu Co., Japan) with a load of 300 gf and a loading time of 15 s. Before testing, coatings were

Table 1. Primers used for RT-PCR–HOB-related markers.

gene	sequence (5′–3′)	melting temperature (°C)
GAPDH	F ACCCAGAAGACTGTGGATGG	60
	R CAGTGAGCTTCCCGTTCAG	
Runx-2	F ATGCTTCATTCGCCTCAC	60
	R ACTGCTTGCAGCCTTAAAT	
OPN	F TTCCAAGTAAGTCCAACGAAAG	60
	R GTGACCAGTTCATCAGATTCAT	
collagen type I	F AGGGTCCCAACGAGATCGAGATCCG	60
	R TACAGGAAGCAGACAGGGCCAACGTCG	
BSP	F ATGGCCTGTGCTTTCTCAATG	60
	R GGATAAAAGTAGGCATGCTTG	

subjected to fine polishing. Hardness values were recorded on 15 different positions. The results are presented as mean ± s.d.

2.3. Ion release and acellular mineralization tests

In order to measure the ion release behaviours of HT and SP coatings, they were immersed for 7 days in a 15 ml sodium chloride solution (pH 7.4) buffered with tris(hydroxymethyl)aminomethane and hydrochloric acid (HCl–Tris-buffered solution). After soaking, pH values of the buffered solution were measured and ion concentrations were tested by inductively coupled plasma atomic emission spectroscopy (ICP-OES, Optima 3000 DV, USA).

The ability of the coatings to induce the precipitation of Ca and phosphorus (P) compounds was evaluated by immersing coatings in cell-free culture medium. Briefly, coatings were sterilized by immersion in 70 per cent ethanol solution overnight, and then washed with phosphate-buffered saline (PBS) before soaking in culture medium. Three millilitres of culture medium was added into each well of 12-well culture plate containing coating samples. The coating samples were incubated at 37°C in a humidified, 5 per cent CO_2 atmosphere for 5 h, and then washed with ultrapure water, dried and carbon-sputtered for SEM observation. The chemical composition of the deposits formed on the coating surface after mineralization was analysed using energy-dispersive spectroscopy (EDS), which was attached to the SEM instrument.

2.4. Isolation and culture of primary human osteoblasts

Permission to use discarded human tissue was granted by the Human Ethics Committee of the University of Sydney and informed consent was obtained. Primary human osteoblasts (HOBs) were isolated from normal human trabecular bone as previously described [34]. Briefly, bone was divided into 1 mm^3 pieces, washed several times in PBS, and digested with 0.02 per cent (w/v) trypsin (Sigma–Aldrich, USA) in PBS, pH 7.4, for 90 min at 37°C. Cells were then cultured in a complete media containing α-minimal essential medium (α-MEM, Gibco Laboratories, USA), supplemented with 10 per cent (v/v) heat-inactivated foetal calf serum (FCS, Gibco Laboratories), 2 mM L-glutamine (Gibco Laboratories), 25 mM Hepes buffer (Gibco Laboratories), 2 mM sodium pyruvate, 30 mg ml^{-1} penicillin, 100 mg ml^{-1} streptomycin (Gibco Laboratories) and 0.1 mM L-ascorbic acid phosphate magnesium salt (Wako Pure Chemicals, Osaka, Japan). Cells were cultured at 37°C in an atmosphere of 5 per cent CO_2 and media were refreshed every three days. Upon confluence, cells were passaged and those at passage 3 were used in the experiments.

2.5. Cell attachment and morphological observation

After the cells reached 80–90% confluence, they were trypsinized using TrypLE Express (Invitrogen), subsequently centrifuged and suspended in complete media to produce a cell suspension with a density of 3.4×10^4 cells per millilitre. Then, a 1 ml cell suspension was added into each well of a 24-well cell culture plate containing coating samples. After culturing for 2, 5 and 24 h, cells were fixed in a 4 per cent paraformaldehyde solution, post-fixed using 1 per cent osmium tetroxide in PBS for 1 h, then dehydrated in a serial of graded ethanol solution (30, 50, 70, 90, 95 and 100%), and finally dried in hexamethyldisilizane for 3 min. The dried coating samples were gold-sputtered prior to SEM observation.

2.6. Cell proliferation assay

The CellTiter 96 Aqueous Assay (Promega, USA), a colorimetric method, was used to determine the number of viable cells. The assay is a combined solution of tetrazolium compound 3-(4,5-dimethylthiazol-2-yl)-5-(3-carboxymethoxyphenyl)-2-(4-sulphophenyl-2H-tetrazolium) (MTS) and an electron coupling reagent (phenazine methosulphate) with a volume ratio of 20 : 1. The former compound can be bioreduced by viable cells into a formazan, which is soluble in cell culture medium. So, the absorbance of the formazan at 490 nm is directly proportional to the number of viable cells. Four samples of each type of coatings were tested for each time point and the uncoated Ti-6Al-4V discs were used as a control. Briefly, 1 ml of cell suspension with a cell density of 8.5×10^4 cell ml^{-1} was added into each well of a 24-well culture plate containing the coating samples. After 3 and 7 days, the culture medium was replaced by 700 µl of the

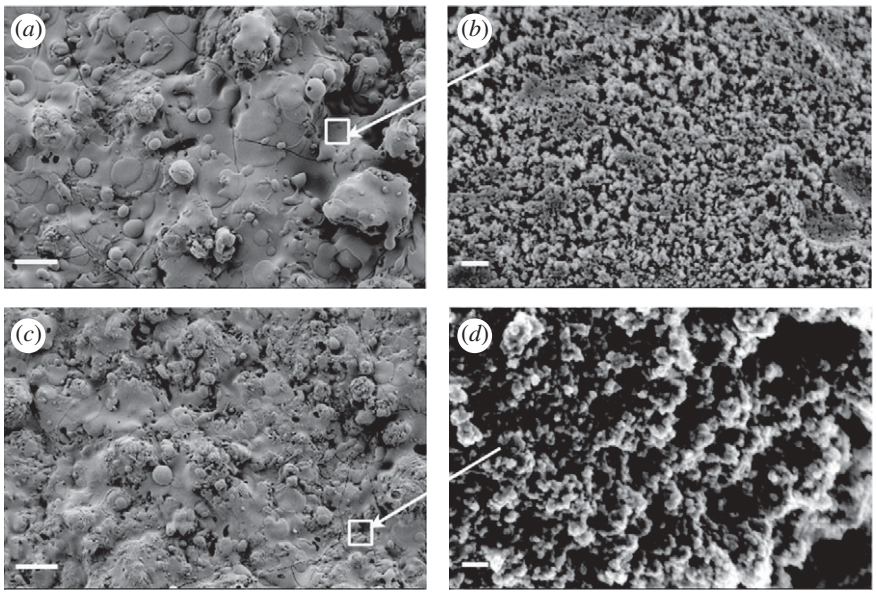

Figure 1. SEM micrographs of the (*a*,*b*) HT and (*c*,*d*) SP coatings. Images (*b*) and (*d*) are under higher magnification. Scale bars, (*a*) 30 μm, (*b*) 200 nm, (*c*) 30 μm and (*d*) 200 nm.

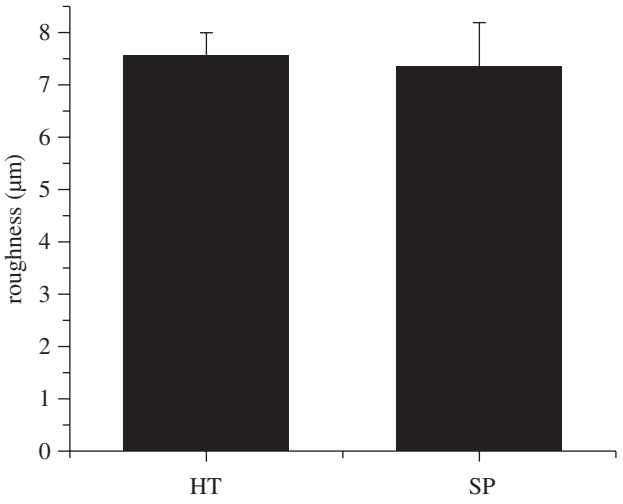

Figure 2. Surface roughnesses of the HT and SP coatings.

MTS working solution which was a five times diluted solution of the CellTiter 96 Aqueous Assay in PBS. After 4 h of further incubation, 100 μl of the working solution was transferred to a 96-well cell culture plate for measuring the absorbance using a microplate reader (PathTech) at 490 nm.

2.7. Quantitative real-time polymerase chain reaction

HOBs were seeded on the coating samples at a cell density of 2×10^4 cell cm^{-2} and cultured for 1 day and 7 days. After each time point, total RNA was isolated from HOBs cultured on coating samples and the control samples of uncoated Ti-6Al-4V discs by using Trizol (Sigma) following the manufacturer's instructions. First-strand cDNA was synthesized from 0.7 μg total RNA using the Omniscript RT Kit (Qiagen, USA) according to manufacturer's instructions. The cDNA was then analysed by real-time PCR (Rotor-Gene 6000, Corbett Life Science) for the osteoblast-related genes: Runx-2, collagen type I, osteopontin (OPN) and bone sialoprotein (BSP) and their relative gene expression levels were obtained by normalizing to glyceraldehyde 3-phosphate dehydrogenase (GAPDH). Primers used for the selected genes are listed in table 1.

2.8. Statistical analysis

The data were obtained from four independent experiments and expressed as mean ± s.d. For statistical analysis, SPSS 17.0 program was used. Levene's test was performed to determine the homogeneity of variance for all the data, and then Tukey HSD *post hoc* tests were used for the data with homogeneous variance, otherwise, Tamhane's T2 *post hoc* was employed. A p-value of less than 0.05 was considered significant.

3. RESULTS

3.1. Phase composition and microstructure of coatings

SEM micrographs of HT and SP coatings are displayed in figure 1. Many splats can be observed on the rough surface of the coatings (figure 1*a*,*c*), which resulted from the impingement of the melted powders on the existing coating layers. Higher magnification views (figure 1*b*,*d*) clearly show the existence of nanostructures on the coating surfaces, with grain sizes less than 50 nm. Surface roughness values (R_a) measured by the surface profilometer are graphed in figure 2 showing that HT and SP coatings have similar R_a values of around 7.5 μm.

XRD patterns of the as-received powders and the as-sprayed coatings are displayed in figure 3. The XRD patterns of the HT and SP powders consist of many sharp peaks corresponding to HT (JCPDS no. 12-0453; figure 3*a*) and SP (JCPDS no. 11-0142; figure 3*b*), indicating that the spray feedstocks are

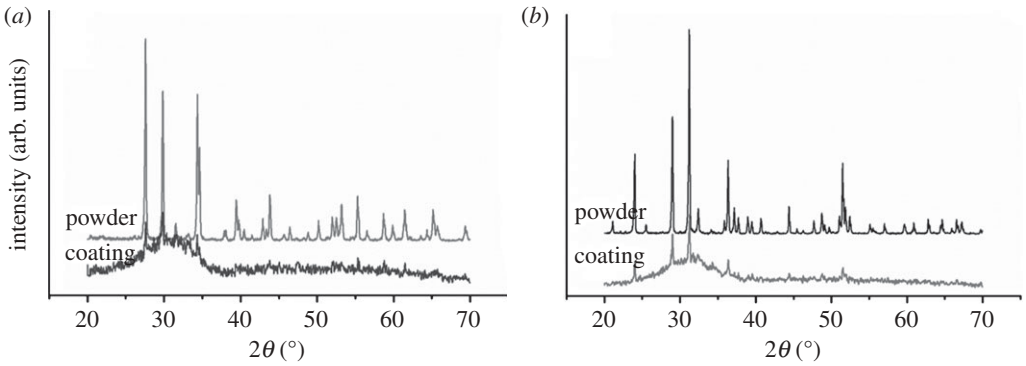

Figure 3. XRD patterns of the (*a*) HT and (*b*) SP powder feedstock as well as the as-sprayed coatings.

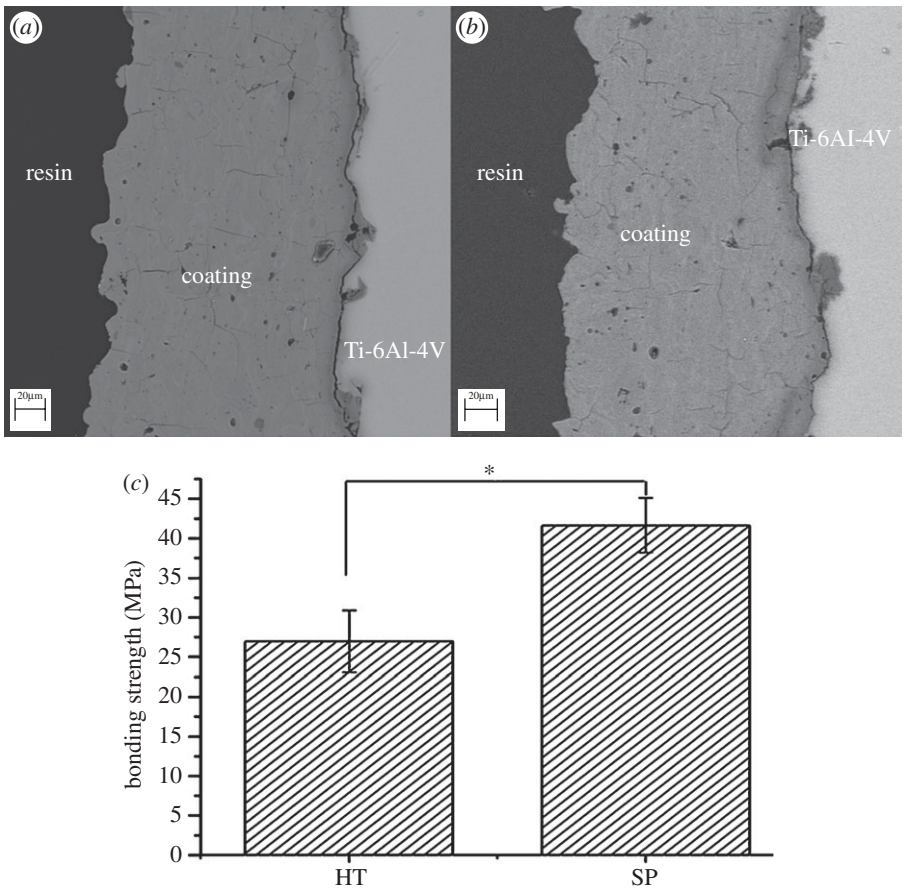

Figure 4. Cross-sectional morphology of the (*a*) HT and (*b*) SP coatings and (*c*) their bonding strength with the Ti-6Al-4V. Asterisk represents significant difference; p-value < 0.05. Scale bars, (*a*,*b*) 20 μm.

single-phase powders with high crystallinity. XRD patterns of the coatings show that some peaks overlapped or disappeared and a glass bulge appeared, but several resolved peaks can still be identified from the bulge loop. This indicates that both HT and SP coatings were mainly composed of glass (amorphous) phases together with certain amount of crystalline phase, and accordingly these coatings were named glass–ceramic coatings.

3.2. Interfacial bonding and nanoindentation

Figure 4 shows the cross-sectional morphology of HT and SP coatings and their bonding strength with Ti-6Al-4V. Compared with HT coatings (figure 4*a*), the interfacial bonding of the SP coatings is better (figure 4*b*). The bonding strength of SP coatings (41.0 ± 3.5 MPa) is significantly higher than that of HT coatings (27.0 ± 3.9 MPa; figure 4*c*).

The values of Vickers hardness of HT and SP coatings are 539.8 ± 60.2 and 567.2 ± 66.5 (Hv), respectively, as shown in figure 5. At a p-value less than 0.05, there are no significant differences in Vickers hardness between these two coatings.

3.3. Ion releases and pH variation

Figure 6 shows the change of the relative content of compositional elements of the HT and SP coatings

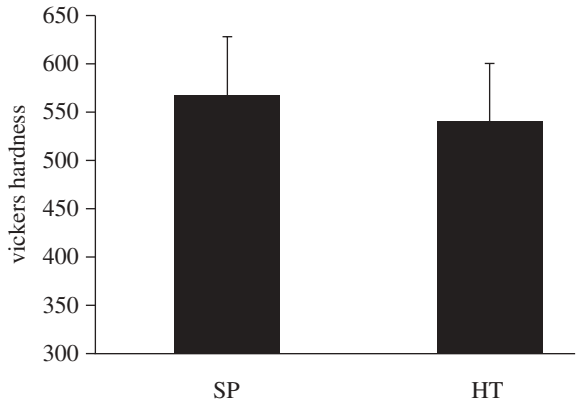

Figure 5. Vickers hardness of the SP and HT coatings. There is no significant difference between HT and SP coatings.

before and after immersion in HCl–Tris-buffered solution for 7 days. After immersion, the relative contents of Si and Zn in the HT coating increased while that of Ca decreased (figure 6*a*). As the buffered solution is free of Si, Ca and Zn, the increase of Si and Zn relative contents is due to the decrease of Ca content in the HT coating. For SP coatings, the variation of the relative contents of Ca and Si before and after immersion was less than that for HT coatings (figure 6*b*), while no significant change in Ti content was found. Figure 6*c* shows a significant increase in the Si/Ca ratio of the HT and SP coatings after immersion in the buffered solution, with the HT coating exhibiting significant increase over the SP coatings, suggesting the greater ability of HT coatings to release Ca ions than Si ions into the buffered solution. Accordingly, a larger variation in pH values of the buffered solution can be observed after the immersion of HT coatings when compared with that seen for SP coatings (figure 6*d*). The released amount of Ca and Si ions from HT coatings after 7 days of immersion in buffered solution is significantly higher ($p < 0.05$) than that from the SP coating (table 2), consistent with the above-mentioned EDS results. In addition, a certain amount of Zn ions was also released from the HT coating, but the release of Ti ions from the SP coating was negligible.

3.4 Acellular mineralization in cell-free culture medium

The surface morphology of the HT coatings after incubation in cell-free medium is shown in figure 7*a*,*b*. After 5 h of incubation, a significant amount of mushroom-like deposits was found on the surface of HT coatings (figure 7*a*,*b*). Figure 7*c*,*d* displays the EDS results of the HT coating before mineralization and the deposits formed on the surface after mineralization. The intensity of Ca peaks largely increased while that of Si largely decreased in the EDS of the deposits (figure 7*d*). The Ca/Si and Ca/Zn ratios of the HT coatings before and after immersion are listed in table 3. Both Ca/Si and Ca/Zn ratios of the deposits are significantly higher than those of HT coatings, suggesting that Ca is one of the main elements of the deposits. Besides those peaks of the compositional elements of the coatings, a P peak with an intensity similar to the Si peak was observed (figure 7*c*), indicating the existence of P in the deposits. In contrast, no deposits were found on the SP coatings after 5 h of incubation in cell-free culture medium. These results indicate that HT coatings can induce Ca and P compound precipitation on their surfaces.

3.5. Cell attachment and proliferation on the coatings

The micrographs showing the attachment and spreading of HOBs cultured on HT and SP coatings for 2, 5 and 24 h are displayed in figure 8. On HT coatings, HOBs had already attached well and started to form extensions to explore coating surfaces after 2 h of incubation (figure 8*a*). By 5 h, cells further spread and became more flattened, and lamellipodia extended from the cytoplasma to interact with the underlying coatings (figure 8*b*). On closer examination, HOBs were seen spanning a depressed area from one elevated area to another by their lamellipodia (figure 8*d*). In addition, some filopodia were observed at the rim of lamellipodia (figure 8*d*, arrows). Similar cell behaviours were observed in HOBs after 24 h of culture (figure 8*c*,*e*). HOBs cultured on SP coatings also exhibited good attachment and spreading (figure 9). However, HOBs on SP coatings exhibited a more elongated but less-flattened morphology at 2 h and 5 h time points (figure 9*a*,*b*). Under higher magnification, lamellipodia could be easily seen extending along the SP coating surfaces, but no obvious filopodia were observed (figure 9*d*,*e*).

The proliferation rates of HOBs on HT and SP coatings were compared with the control (Ti-6Al-4V disc). The results showed that HOB proliferation rate on HT coatings was highest ($p < 0.05$) when compared with those on SP coatings and Ti-6Al-4V disc after 7 days (figure 10). Cells on the SP coatings showed a slow proliferation rate in the initial 3 days of culture, which increased thereafter, and reached a similar level to that of Ti-6Al-4V discs on day 7. These results imply that HOBs can proliferate well on HT and SP coatings.

3.6. Quantitative real-time polymerase chain reaction

Figure 11 shows the expression levels of bone-related genes (Runx-2, OPN, type I collagen and BSP) in relation to the house-keeping gene (GAPDH) after 1 and 7 days of culture. At 1 day, Runx-2 mRNA gene expression was higher in HOBs cultured on the SP coatings and Ti-6Al-4V discs, compared with that on HT coatings. At 7 days, Runx-2 expression level on HT coatings caught up with that on Ti-6Al-4V, while HOBs on SP coatings showed the highest Runx-2 expression level (figure 11*a*). No significant differences in BSP gene expression were found in HOBs cultured on HT and SP coatings, and Ti-6Al-4V discs at both time points (figure 11*b*). OPN gene expression level in HOBs on both types of coatings, especially on HT coatings, was higher than that on Ti-6Al-4V discs at both time points (figure 11*c*). Higher expression levels of type I collagen were observed in HOBs cultured

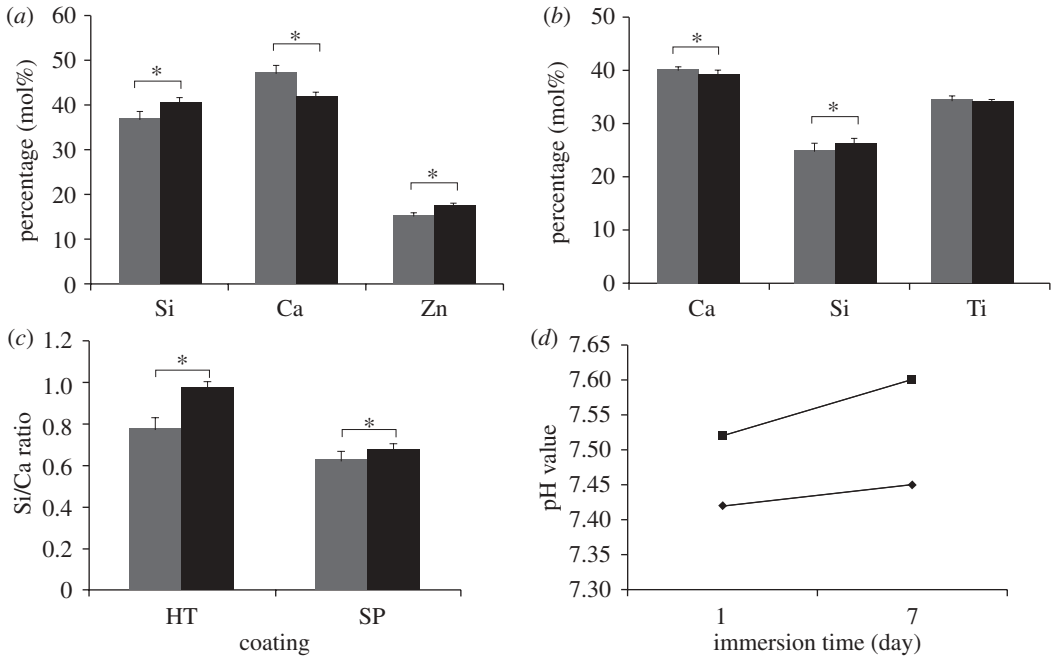

Figure 6. Variation of the relative percentage of compositional elements of (*a*) HT and (*b*) SP coatings, (*c*) their Si/Ca molar ratio and (*d*) pH value changes of HCl–Tris-buffered solution after the immersion of coatings. Asterisk represents significant difference; p-value < 0.05. (*a–c*) Grey bars represent before immersion and black bars represent after immersion and (*d*) filled diamonds represent SP and filled squares represent HT.

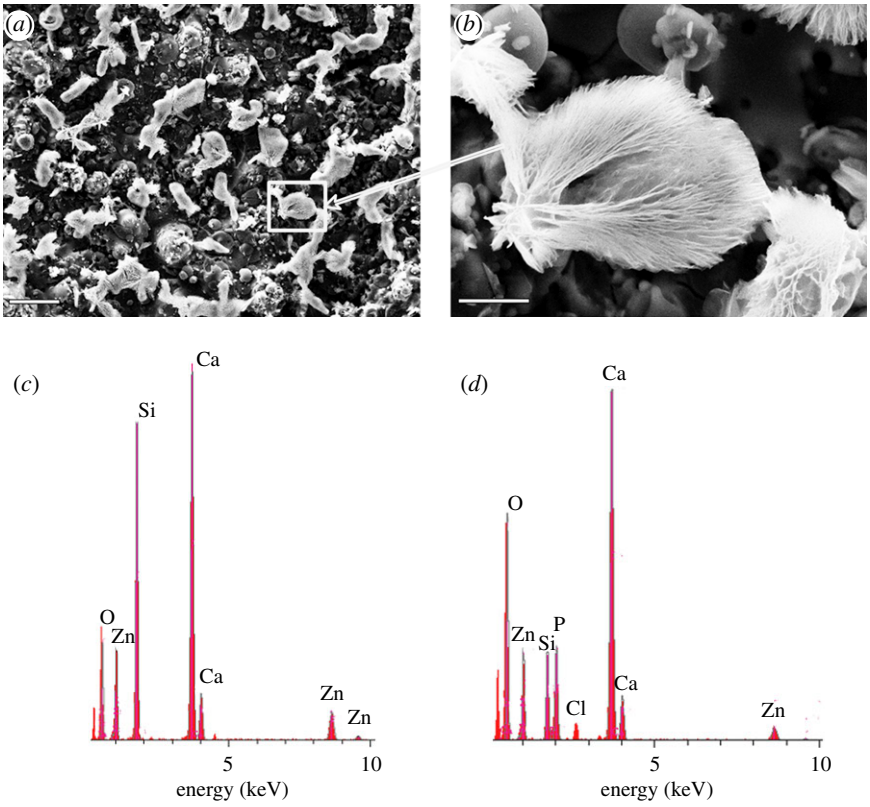

Figure 7. Surface morphology of (*a*,*b*) the HT coatings after incubation in cell-free culture medium for 5 h and the EDS of (*c*) the HT coating before incubation and (*d*) the deposits on its surface after incubation. Scale bars, (*a*) 50 μm and (*b*) 10 μm. (Online version in colour.)

on both coatings, compared with Ti-6Al-4V discs at day 7 (figure 11*d*). Collectively, these data indicate that both HT and SP coatings support the differentiation of HOBs.

4. DISCUSSION

In this work, HT and SP coatings were fabricated using atmospheric plasma spray technique. Both types of

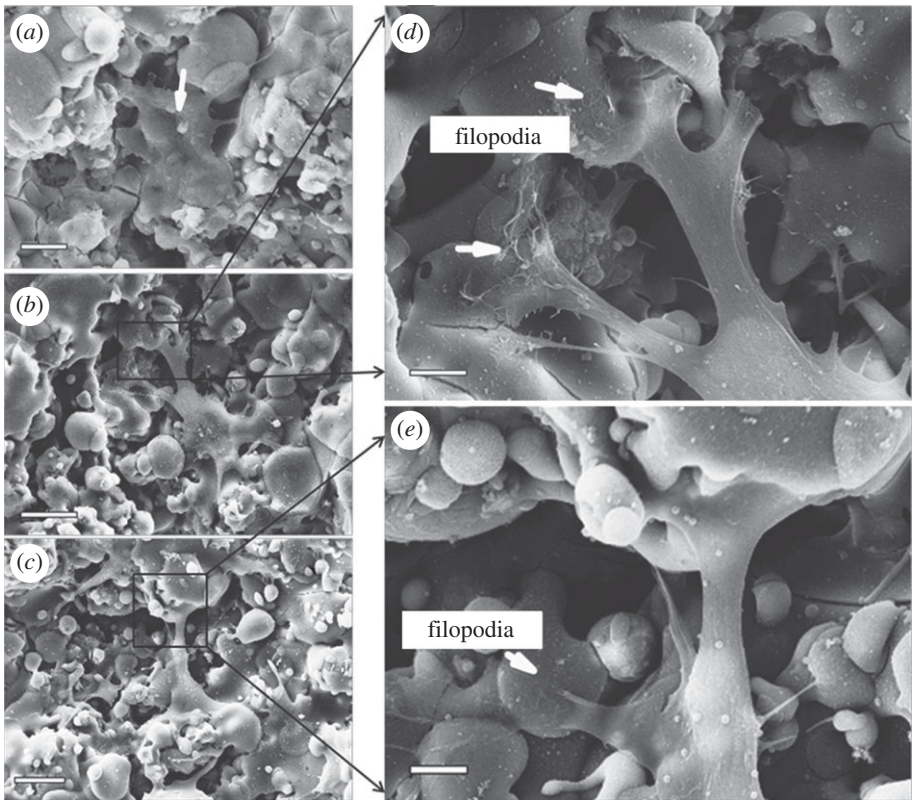

Figure 8. SEM micrographs of HOBs cultured on the HT coatings for (*a*) 2 h, (*b*,*d*) 5 h and (*c*,*e*) 1 day. Scale bars, (*a*) 10 μm, (*b*,*c*) 20 μm and (*d*,*e*) 5 μm.

Table 2. Concentrations of ions released in the HCl–Tris-buffered solution from the HT and SP coatings after 7 days of immersion.

coatings	Ca (ppm)	Si (ppm)	Zn (ppm)	Ti (ppm)
HT	107.41	13.09	0.90	0
SP	9.40	1.54	0	0.014

Table 3. Ca/Si and Ca/Zn ratios of the as-sprayed HT coating and the deposits formed on its surface after incubation in cell-free culture medium for 5 h.

	Ca/Si ratio	Ca/Zn ratio
HT coating before mineralization	1.23 ± 0.06	3.06 ± 0.14
deposits on HT coating after mineralization	5.38 ± 0.25	8.44 ± 0.41

coatings exhibited glass–ceramic structure and had nanostructured surfaces due to the high temperature and the super-high cooling rate of the plasma spray process [3,35,36]. The bonding strength of SP coating was superior to that of HT coating; and both were higher compared with the reported values of plasma-sprayed HAp coating [37–39]. Coefficient of thermal expansion is an important factor influencing the quality of the coatings including the formation of cracks, residual stress and bonding strength. The coefficients of HT and SP ceramics and Ti-6Al-4V alloy were reported to be $11.2 \times 10^{-6}\,K^{-1}$ [24], $6 \times 10^{-6}\,K^{-1}$ and $8.4–8.8 \times 10^{-6}\,K^{-1}$ [15], respectively, while that of HAp coatings is around $15.2 \times 10^{-6}\,K^{-1}$ [40]. The close match of the coefficients of thermal expansion of the HT and SP coatings to that of Ti-6Al-4V alloy contributed to their higher bonding strength compared with HAp coatings. The superior bonding strength of the SP compared to HT coatings is possibly due to the presence of Ti in the SP coating which may enhance the chemical and diffusion bonding between SP coatings and the underlying Ti-6Al-4V [41]. Zheng *et al.* [39] demonstrated that the bonding strength of the plasma-sprayed HAp coatings was greatly improved using mixed powder feedstock of Ti and HAp. Besides bonding strength, hardness is another important parameter for biomedical coatings as it affects their anti-wear properties. The hardness of our developed coatings was higher compared with those of thermal sprayed HAp despite that our coatings were tested under higher load, as can be seen in table 4. Actually, the hardness of these two coatings is also comparable to those of HAp ceramic blocks (also seen in table 4).

Acellular mineralization studies suggest that HT coatings could induce the formation of Ca and P compounds on their surfaces after immersion in cell-free culture medium for 5 h. The mechanism of Ca and P compound formation on HT coatings is similar to that of $CaO–SiO_2$-based bioglass and bioactive glass–ceramic [21]. Firstly, the increase in Ca ions may result in the culture medium being more supersaturated with respect to the Ca and P compounds, thus favouring their precipitation on the coating surface. Secondly,

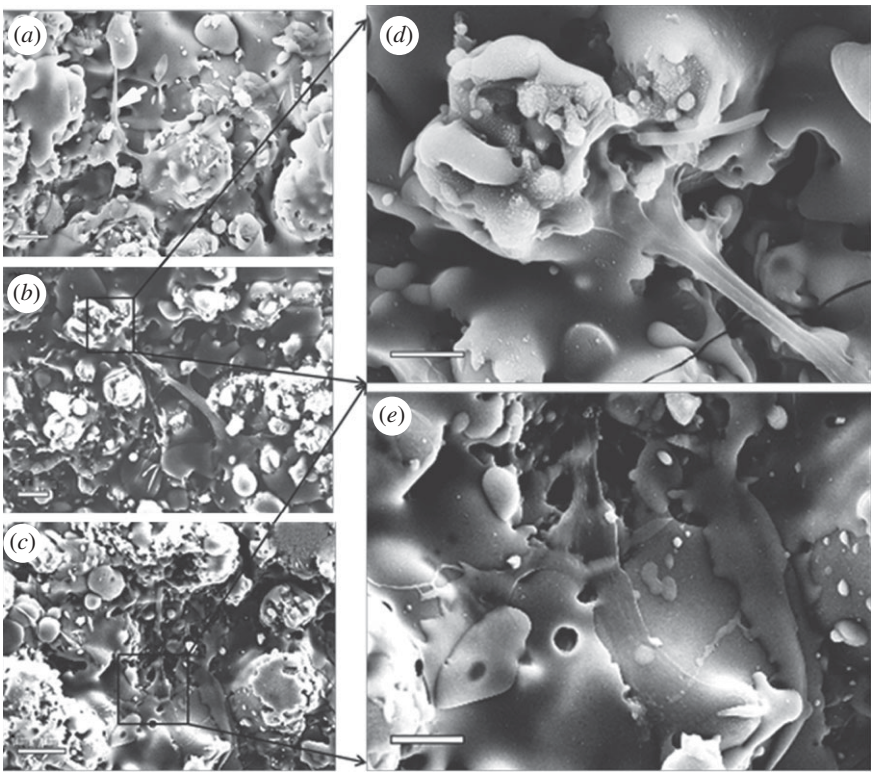

Figure 9. SEM micrographs of HOBs cultured on the SP coatings for (*a*) 2 h, (*b*,*d*) 5 h and (*c*,*e*) 1 day. Scale bars, (*a*,*b*,*e*) 10 μm, (*c*) 20 μm and (*d*) 5 μm.

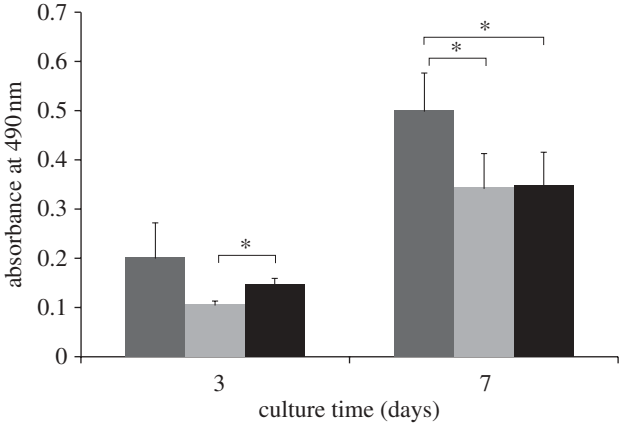

Figure 10. HOB proliferation on HT and SP coatings after culturing for 3 and 7 days. Ti-6Al-4V was used as a control. Asterisk represents significant difference; p-value < 0.05. Dark grey bars represent HT, light grey bars represent SP and black bars represent Ti alloy.

the faster release rate of Ca, compared with that of Si ions (figure 6*a*–*c*), may result in the formation of Si–OH groups having the ability to induce Ca and P precipitation [48]. Compared with HT coatings, less Si and Ca ions were released from SP coatings, which was possibly the reason for the failure of Ca and P compound precipitation on SP coatings. Although HT coatings have high ability to release Ca and Si ions compared with SP coatings, the released amount is far less than that from $CaO–SiO_2$ materials [22,23,27,49,50]. In addition, the stability of HT coatings can be contributed by two factors: firstly, the slower release of Si compared with Ca ions can maintain the SiO_2 networks for a longer time; secondly, the faster precipitation of Ca and P compounds can compensate for the release of Ca ions and may hinder further release of Ca and Si.

HOBs attach, spread, proliferate and differentiate well on both types of coatings indicating their good biocompatibility. It is well known that cell behaviours are strongly influenced by both topographical and chemical cues. Topographically, HT and SP coatings prepared in this study possessed both micro- and nano-sized topographies. The positive effects of micron-sized roughness on the attachment, proliferation and differentiation have been well documented [51,52]. The effect of nanostructured surface of biomaterials on osteoblast behaviours has been widely studied. Webster *et al.* [33] showed that the critical grain size for enhanced osteoblast adhesion was 49–67 nm for Al_2O_3 ceramics and 32–56 nm for TiO_2 ceramics. In this work, both HT and SP coatings possessed nanostructured surfaces with grain sizes of less than 50 nm and micro-sized topographies, which are thought to contribute to their biocompatibility. Besides topographical cues, the released ions also contribute to the good biocompatibility of HT and SP coatings. Studies reported that ion dissolution products (Si and Ca in particular) of $CaO–SiO_2$-based bioactive materials stimulate osteoblast proliferation and differentiation [18–20,53]. Ni *et al.* [53] demonstrated that cell attachment, proliferation of osteoblast-like cells and the expression level of ALP activity were greater on the surface of $CaSiO_3$ ceramics than on β-TCP ceramics. The key determining factor for these differences is thought to be the Si ions and the higher amount of

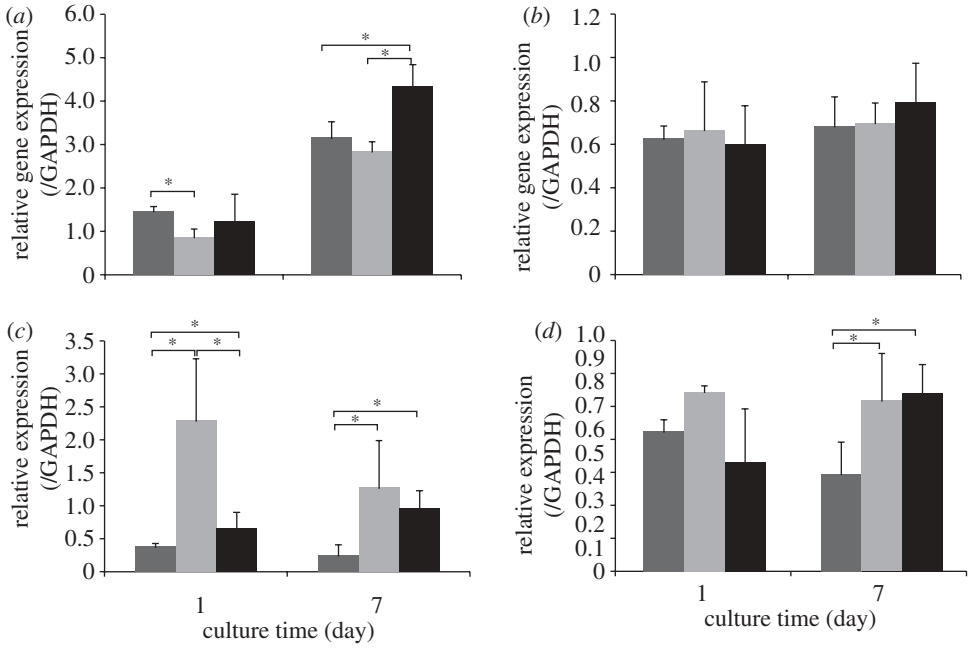

Figure 11. Bone-related gene expression levels of HOBs cultured on HT and SP coatings determined by qRT-PCR; Ti alloy was used as a control. (*a*) Runx-2, (*b*) BSP, (*c*) OPN and (*d*) collagen I. Asterisk represents significant difference; p-value < 0.05. Dark grey bars represent Ti alloy, light grey bars represent HT coating and black bars represent SP coating.

Table 4. Summary of the hardness values of thermal sprayed hydroxyapatite coatings and ceramic blocks. APS, atmosphere plasma spraying; GTPS, gas tunnel type plasma spraying; HVSFS, high-velocity suspension flame spraying. Asterisks represent not available in the literature.

		test conditions			
existing form	fabrication method	load (g)	load time (s)	Vickers hardness (Hv)	references
coating	APS	50	15	253–437	[42]
coating	GTPS	50	20	420–460	[43]
coating	APS	50	15	200–310	[44]
coating	HVSFS	10	*	266–389	[45]
coating	APS	10	*	283–323	[45]
block	high temperature sintering (1050°C)	200	*	418	[46]
block	high temperature sintering (1000–1450°C)	200	10	119–620	[47]

Ca ions released from $CaSiO_3$ ceramics than β-TCP ceramics [53]. Sun *et al.* [18] reported that Ca and Si ions released from plasma-sprayed Ca_2SiO_4 coatings enhanced the expression of osteoblast differentiation markers including alkaline phosphatase, osteocalcin and type I collagen. Therefore, it is plausible to suggest that the enhanced HOB differentiation seen on the HT and SP coatings is due to the release of Ca and Si ions from the coatings. Compared with the difference in mineralization ability of HT and SP coatings, the required amount of Ca and Si ions for inducing the expression of bone-related genes appears to be less than that required for faster acellular mineralization ability.

The higher proliferation rate of HOBs cultured on HT coatings compared with SP coatings may be attributed to the Zn ions released from the HT coatings. Previous work by Ramaswamy *et al.* [54] demonstrated that cell proliferation rate on HT ceramics was higher than that on $CaSiO_3$ ceramics despite the fact that Ca and Si ions released from $CaSiO_3$ ceramics were significantly higher than that from HT ceramics, suggesting that the released Zn ions might be responsible for the higher cell proliferation rate. It was reported that Zn influences cell proliferation by directly regulating DNA synthesis and influencing hormonal regulation of cell division [48,55]. Furthermore, Zn is essential for maintaining the IGF-I level for cell proliferation [55]. Therefore, it is plausible to attribute the faster cell proliferation observed on the HT coatings to the presence of Zn ions in the surrounding environment. In summary, data obtained in this study indicated that both HT and SP coatings exhibit potentials for orthopaedic application. In our next work, an *in vivo* animal model will be used to further investigate the *in vivo* bone fixation ability of these two types of coatings.

5. CONCLUSIONS

Glass–ceramic HT and SP coatings were successfully fabricated using atmospheric plasma spray techniques. Both types of coatings have a nanostructured surface with grains less than 50 nm in size. Their bonding strength is higher than that of plasma-sprayed HAp coatings and their hardness is higher compared with Ti-6Al-4V alloys and HAp coatings. Both types of coatings can support HOB cell attachment, spreading and proliferation on their surfaces and are capable of enhancing the expression of bone-related genes, which is ascribed to the Ca and Si ions released from the coatings. Additionally, HOBs on HT coatings exhibit a higher proliferation rate than SP coatings and Ti-6Al-4V alloys, which is thought to be related to the release of Zn ions from the HT coatings.

The authors acknowledge the Australia National Health and Medical Research Council, Rebecca Cooper Foundation and the Australian Research Council. They thank Jeffrey Shi and Linda Wang (Chemical Engineering of University of Sydney) for their help in the ICP-OES tests.

REFERENCES

1 Niinomi, M. 2008 Metallic biomaterials. *J. Artif. Organs* **11**, 105–110. (doi:10.1007/s10047-008-0422-7)
2 Gomez-Vega, J. M., Saiz, E. & Tomsia, A. P. 1999 Glass-based coatings for titanium implant alloys. *J. Biomed. Mater. Res.* **46**, 549–559. (doi:10.1002/(SICI)1097-4636(19990915)46:4<549::AID-JBM13>3.0.CO;2-M)
3 Liu, X., Chu, P. K. & Ding, C. 2004 Surface modification of titanium, titanium alloys, and related materials for biomedical applications. *Mater. Sci. Eng. R* **47**, 49–121. (doi:10.1016/j.mser.2004.11.001)
4 Zuruzi, A. S., Ward, M. S. & MacDonald, N. C. 2005 Fabrication and characterization of patterned micrometre scale interpenetrating Au–TiO_2 network nanocomposites. *Nanotechnology* **16**, 1029–1034. (doi:10.1088/0957-4484/16/8/005)
5 Wong, M., Eulenberger, J., Schenk, R. & Hunziker, E. 1995 Effect of surface topology on the osseointegration of implant materials in trabecular bone. *J. Biomed. Mater. Res.* **29**, 1567–1575. (doi:10.1002/jbm.820291213)
6 Amstutz, H. C., Campbell, P., Kossovsky, N. & Clarke, I. C. 1992 Mechanism and clinical significance of wear debris-induced osteolysis. *Clin. Ortho. Related Res.* **276**, 7–18. (doi:10.1097/00003086-199203000-00003)
7 De Aza, P. N., Fernández-Pradas, J. M. & Serra, P. 2004 In vitro bioactivity of laser ablation pseudowollastonite coating. *Biomaterials* **25**, 1983–1990. (doi:10.1016/j.biomaterials.2003.08.036)
8 Kitsugi, T., Nakamura, T., Oka, M., Senaha, Y., Goto, T. & Shibuya, T. 1996 Bone-bonding behavior of plasma-sprayed coatings of Bioglass®, AW–glass ceramic, and tricalcium phosphate on titanium alloy. *J. Biomed. Mater. Res.* **30**, 261–269. (doi:10.1002/(SICI)1097-4636(199602)30:2<261::AID-JBM17>3.0.CO;2-P)
9 Kokubo, T., Kushitani, H., Ohtsuki, C., Sakka, S. & Yamamuro, T. 1992 Chemical reaction of bioactive glass and glass–ceramics with a simulated body fluid. *J. Mater. Sci. Mater. Med.* **3**, 79–83. (doi:10.1007/BF00705272)
10 Kokubo, T., Kushitani, H., Sakka, S., Kitsugi, T. & Yamamuro, T. 1990 Solutions able to reproduce *in vivo* surface-structure changes in bioactive glass–ceramic A-W[3]. *J. Biomed. Mater. Res.* **24**, 721–734. (doi:10.1002/jbm.820240607)
11 Liu, X., Morra, M., Carpi, A. & Li, B. 2008 Bioactive calcium silicate ceramics and coatings. *Biomed. Pharmacother.* **62**, 526–529. (doi:10.1016/j.biopha.2008.07.051)
12 Leatherman, B. D. & Dornhoffer, J. L. 2002 Bioactive glass ceramic particles as an alternative for mastoid obliteration: results in an animal model. *Otol. Neurotol.* **23**, 657–660.
13 Vogel, M., Voigt, C., Gross, U. M. & Müller-Mai, C. M. 2001 In vivo comparison of bioactive glass particles in rabbits. *Biomaterials* **22**, 357–362. (doi:10.1016/s0142-9612(00)00191-5)
14 Bloyer, D. R., Gomez-Vega, J. M., Saiz, E., McNaney, J. M., Cannon, R. M. & Tomsia, A. P. 1999 Fabrication and characterization of a bioactive glass coating on titanium implant alloys. *Acta Mater.* **47**, 4221–4224. (doi:10.1016/s1359-6454(99)00280-3)
15 Wu, C., Ramaswamy, Y., Gale, D., Yang, W., Xiao, K., Zhang, L., Yin, Y. & Zreiqat, H. 2008 Novel sphene coatings on Ti-6Al-4V for orthopedic implants using sol–gel method. *Acta Biomater.* **4**, 569–576. (doi:10.1016/j.actbio.2007.11.005)
16 Gomez-Vega, J. M., Saiz, E., Tomsia, A. P., Marshall, G. W. & Marshall, S. J. 2000 Bioactive glass coatings with hydroxyapatite and Bioglass® particles on Ti-based implants. 1. Processing. *Biomaterials* **21**, 105–111. (doi:10.1016/s0142-9612(99)00131-3)
17 Silver, I. A., Deas, J. & Erecinska, M. 2001 Interactions of bioactive glasses with osteoblasts in vitro: effects of 45S5 Bioglass®, and 58S and 77S bioactive glasses on metabolism, intracellular ion concentrations and cell viability. *Biomaterials* **22**, 175–185. (doi:10.1016/s0142-9612(00)00173-3)
18 Sun, J., Wei, L., Liu, X., Li, J., Li, B., Wang, G. & Meng, F. 2009 Influences of ionic dissolution products of dicalcium silicate coating on osteoblastic proliferation, differentiation and gene expression. *Acta Biomater.* **5**, 1284–1293. (doi:10.1016/j.actbio.2008.10.011)
19 Valerio, P., Pereira, M. M., Goes, A. M. & Leite, M. F. 2004 The effect of ionic products from bioactive glass dissolution on osteoblast proliferation and collagen production. *Biomaterials* **25**, 2941–2948. (doi:10.1016/j.biomaterials.2003.09.086)
20 Xynos, I. D., Edgar, A. J., Buttery, L. D. K., Hench, L. L. & Polak, J. M. 2001 Gene-expression profiling of human osteoblasts following treatment with the ionic products of Bioglass® 45S5 dissolution. *J. Biomed. Mater. Res.* **55**, 151–157. (doi:10.1002/1097-4636 20010555:2<151::AID-JBM1001>3.0.CO;2-D)
21 Hench, L. 2006 The story of Bioglass®. *J. Mater. Sci. Mater. Med.* **17**, 967–978. (doi:10.1007/s10856-006-0432-z)
22 Wu, C., Chang, J. & Zhai, W. 2005 A novel hardystonite bioceramic: preparation and characteristics. *Ceram. Int.* **31**, 27–31. (doi:10.1016/j.ceramint.2004.02.008)
23 Wu, C., Ramaswamy, Y., Soeparto, A. & Zreiqat, H. 2008 Incorporation of titanium into calcium silicate improved their chemical stability and biological properties. *J. Biomed. Mater. Res. A* **86**, 402–410. (doi:10.1002/jbm.a.31623)
24 Haussühl, S. & Liebertz, J. 2004 Elastic and thermoelastic properties of synthetic $Ca_2MgSi_2O_7$ (åkermanite) and $Ca_2ZnSi_2O_7$ (hardystonite). *Phys. Chem. Miner.* **31**, 565–567.
25 Wu, C., Ramaswamy, Y., Liu, X., Wang, G. & Zreiqat, H. 2009 Plasma-sprayed $CaTiSiO_5$ ceramic coating on Ti-6Al-4V with excellent bonding strength, stability and cellular bioactivity. *J. R. Soc. Interface* **6**, 159–168. (doi:10.1098/rsif.2008.0274)

26 Tulyaganov, D. U., Agathopoulos, S., Ventura, J. M., Karakassides, M. A., Fabrichnaya, O. & Ferreira, J. M. F. 2006 Synthesis of glass–ceramics in the CaO-MgO-SiO_2 system with B_2O_3, P_2O_5, Na_2O and CaF_2 additives. *J. Eur. Ceram. Soc.* **26**, 1463–1471. (doi:10.1016/j.jeur ceramsoc.2005.02.009)

27 Xue, W., Liu, X., Zheng, X. & Ding, C. 2005 Dissolution and mineralization of plasma-sprayed wollastonite coatings with different crystallinity. *Surf. Coat. Technol.* **200**, 2420–2427. (doi:10.1016/j.surfcoat.2004.07.114)

28 Bolelli, G., Cannillo, V., Lusvarghi, L., Manfredini, T., Siligardi, C., Bartuli, C., Loreto, A. & Valente, T. 2005 Plasma-sprayed glass–ceramic coatings on ceramic tiles: microstructure, chemical resistance and mechanical properties. *J. Eur. Ceram. Soc.* **25**, 1835–1853. (doi:10.1016/j.jeurceramsoc.2004.06.018)

29 Sampath, S. 1993 Microstructural characteristics of plasma spray consolidated amorphous powders. *Mater. Sci. Eng. A* **167**, 1–10. (doi:10.1016/0921-5093(93) 90330-h)

30 Liu, X., Zhao, X., Fu, R. K. Y., Ho, J. P. Y., Ding, C. & Chu, P. K. 2005 Plasma-treated nanostructured TiO_2 surface supporting biomimetic growth of apatite. *Biomaterials* **26**, 6143–6150. (doi:10.1016/j.biomaterials.2005.04.035)

31 Wang, G., Liu, X., Gao, J. & Ding, C. 2009 *In vitro* bioactivity and phase stability of plasma-sprayed nanostructured 3Y-TZP coatings. *Acta Biomater.* **5**, 2270–2278. (doi:10.1016/j.actbio.2009.01.023)

32 Wang, G., Meng, F., Ding, C., Chu, P. K. & Liu, X. 2010 Microstructure, bioactivity and osteoblast behavior of monoclinic zirconia coating with nanostructured surface. *Acta Biomater.* **6**, 990–1000. (doi:10.1016/j.actbio.2009.09.021)

33 Webster, T. J., Siegel, R. W. & Bizios, R. 1999 Osteoblast adhesion on nanophase ceramics. *Biomaterials* **20**, 1221–1227. (doi:10.1016/s0142-9612(99)00020-4)

34 Zreiqat, H. *et al.* 2010 The incorporation of strontium and zinc into a calcium–silicon ceramic for bone tissue engineering. *Biomaterials* **31**, 3175–3184. (doi:10.1016/j.biomaterials.2010.01.024)

35 Liu, C. S., Zhu, Z. G., Xia, J. C. & Sun, D. Y. 2001 Cooling rate dependence of structural properties of aluminium during rapid solidification. *J. Phys. Condens. Matter* **13**, 1873–1890. (doi:10.1088/0953-8984/13/9/311)

36 Sampath, S. & Herman, H. 1996 Rapid solidification and microstructure development during plasma spray deposition. *J. Therm. Spray Technol.* **5**, 445–456. (doi:10.1007/BF02645275)

37 Kweh, S. W. K., Khor, K. A. & Cheang, P. 2002 An in vitro investigation of plasma-sprayed hydroxyapatite (HA) coatings produced with flame-spheroidized feedstock. *Biomaterials* **23**, 775–785. (doi:10.1016/s0142-9612(01)00183-1)

38 Tsui, Y. C., Doyle, C. & Clyne, T. W. 1998 Plasma-sprayed hydroxyapatite coatings on titanium substrates Part 2: optimisation of coating properties. *Biomaterials* **19**, 2031–2043. (doi:10.1016/s0142-9612(98)00104-5)

39 Zheng, X., Huang, M. & Ding, C. 2000 Bond strength of plasma-sprayed hydroxyapatite/Ti composite coatings. *Biomaterials* **21**, 841–849. (doi:10.1016/s0142-9612(99)00255-0)

40 Xue, W., Liu, X., Zheng, X. & Ding, C. 2004 Plasma-sprayed diopside coatings for biomedical applications. *Surf. Coat. Technol.* **185**, 340–345. (doi:10.1016/j.surfcoat.2003.12.018)

41 Pilous, V. & Musil, J. 1988 Bonding of plasma-sprayed coatings with the substrate materials. *Welding Int.* **2**, 934–938. (doi:10.1080/09507118809447582)

42 Mancini, C. E., Berndt, C. C., Sun, L. & Kucuk, A. 2001 Porosity determinations in themally sprayed hydroxyapatite coatings. *J. Mater. Sci.* **36**, 3891–3896. (doi:10.1023/A:1017905818479)

43 Morks, M. F. & Kobayashi, A. 2007 Effect of gun current on the microstructure and crystallinity of plasma-sprayed hydroxyapatite coatings. *Appl. Surf. Sci.* **253**, 7136–7142. (doi:10.1016/j.apsusc.2007.02.183)

44 Mohammadi, Z., Ziaei-Moayyed, A. A. & Sheikh-Mehdi Mesgar, A. 2007 Adhesive and cohesive properties by indentation method of plasma-sprayed hydroxyapatite coatings. *Appl. Surf. Sci.* **253**, 4960–4965. (doi:10.1016/j.apsusc.2006.11.002)

45 Gadow, R., Killinger, A. & Stiegler, N. 2010 Hydroxyapatite coatings for biomedical applications deposited by different thermal spray techniques. *Surf. Coat. Technol.* **205**, 1157–1164. (doi:10.1016/j.surfcoat.2010.03.059)

46 Ioku, K., Yoshimura, M. & Sōmiya, S. 1990 Microstructure and mechanical properties of hydroxyapatite ceramics with zirconia dispersion prepared by post-sintering. *Biomaterials* **11**, 57–61. (doi:10.1016/0142-9612(90)90053-S)

47 Muralithran, G. & Ramesh, S. 2000 The effects of sintering temperature on the properties of hydroxyapatite. *Ceram. Int.* **26**, 221–230. (doi.10.1016/S0272-8842(99)00046-2)

48 Dalby, M. J., McCloy, D., Robertson, M., Wilkinson, C. D. W. & Oreffo, R. O. C. 2006 Osteoprogenitor response to defined topographies with nanoscale depths. *Biomaterials* **27**, 1306–1315. (doi:10.1016/j.biomaterials.2005.08.028)

49 Liang, Y., Xie, Y., Ji, H., Huang, L. & Zheng, X. 2010 Excellent stability of plasma-sprayed bioactive $Ca_3ZrSi_2O_9$ ceramic coating on Ti-6Al-4V. *Appl. Surf. Sci.* **256**, 4677–4681. (doi:10.1016/j.apsusc.2010.02.071)

50 Liu, X., Tao, S. & Ding, C. 2002 Bioactivity of plasma-sprayed dicalcium silicate coatings. *Biomaterials* **23**, 963–968. (doi:10.1016/s0142-9612(01)00210-1)

51 Zhao, G., Raines, A. L., Wieland, M., Schwartz, Z. & Boyan, B. D. 2007 Requirement for both micron- and submicron scale structure for synergistic responses of osteoblasts to substrate surface energy and topography. *Biomaterials* **28**, 2821–2829. (doi:10.1016/j.biomaterials.2007.02.024)

52 Zhu, X., Chen, J., Scheideler, L., Altebaeumer, T., Geis-Gerstorfer, J. & Kern, D. 2004 Cellular reactions of osteoblast to micron- and submicron-scale porous structures of titanium surfaces. *Cells Tissues Organs* **178**, 13–22. (doi:10.1159/000081089)

53 Ni, S., Chang, J., Chou, L. & Zhai, W. 2007 Comparison of osteoblast-like cell responses to calcium silicate and tricalcium phosphate ceramics *in vitro*. *J. Biomed. Mater. Res. B* **80B**, 174–183. (doi:10.1002/jbm.b.30582)

54 Ramaswamy, Y., Wu, C., Zhou, H. & Zreiqat, H. 2008 Biological response of human bone cells to zinc-modified Ca-Si-based ceramics. *Acta Biomater.* **4**, 1487–1497. (doi:10.1016/j.actbio.2008.04.014)

55 MacDonald, R. S. 2000 The role of zinc in growth and cell proliferation. *J. Nutr.* **130**, 1500S–1508S.